*Kovove Mater. 51 2013 373–381*
*DOI: 10.4149/km_2013_6_373*



# The role of $TiB_2$, $Fe_2B$ reinforcements on the wear rate of the coated AISI 430 stainless steel surface by PTA

T. Teker*

*University of Adıyaman, Faculty of Engineering, Department of Materials Engineering, 02040, Adıyaman, Turkey*

Received 11 June 2012, received in revised form 25 September 2012, accepted 25 September 2012

**Abstract**

In-situ synthesized $TiB_2$, $Fe_2B$ reinforced coating was fabricated on AISI 430 steel substrate by using plasma transfer arc (PTA) and FeB, FeTi, FeW powders. The effects of powder type and powder ratio on the wear rate of coating were investigated experimentally. SEM, EDS and XRD analyses were used to differentiate the effect of coating parameters on the microstructure, which characterize the coated surfaces. Primary ferrite ($\alpha$) phase and complex $TiB_2$, $Fe_2B$ borides were detected on the subsurface microstructure. Abrasive wear tests were performed on the coated surface of specimens to examine the influence of the size-vol.% of borides and microstructural changes on the wear rate. Depending on the results, it is seen that the specimens coated by (FeB-FeTi-FeW) ferro-alloy powders mixture have the lowest wear rate.

K e y w o r d s: PTA, surface coating, wear

## 1. Introduction

The plasma transferred arc (PTA) surfacing process is characterized by extremely high temperatures, excellent arc stability, low thermal distortion of the part, and high coating speed [1]. The PTA process has an advantage of using two independent arcs (i.e., non-transferred arc as pilot and transferred arc as main arc). This advantage may play a role in allowing proper microstructural development, and is used in the present study to investigate its effect on the resulting coating properties. Argon gas passing through an inert annulus between the cathode and anode is ionized, forming a constricted plasma arc column. This ionized gas provides a current path for transferred arc [2]. PTA process is widely used for the surface treatment of materials and developed as a modification of the plasma arc welding method [2]. Fe-based metal matrix composites have extensive applications in tools, dies and wear as well as high temperature oxidation resistance components. Ferrous matrix composites have a wide range of applications because of the combination of high mechanical strength. Serious techniques are used to produce high performance composites to improve the interfacial compatibility and to avoid serious interfacial reactions.

In-situ technique is being used as a new technique for productions of ceramic particle reinforced metal matrix composites (MMCs) [3, 4]. In-situ processing technique depends on a basic principle. Thermodynamically stable phases are formed by an exothermal reaction between elements and compounds within the metal matrix. This process has some advantages; the reinforced surface generated in-situ tends to remain free of contamination, such as gas absorption, oxidation and other detrimental surface reactions. The mentioned advantages produce an improved reinforcement matrix interface bond. In addition, the composites produced by the in-situ process exhibit improved mechanical strength, hardness as well as enhanced wear resistance [5, 6].

Titanium diboride ($TiB_2$) is the most inert, stiff, and hardest of all the borides [7], and has high mechanical strength and high resistance to wear and high tensile strength at high temperatures. In contrast to most ceramics, it is electrically and thermally conductive [7, 8]. These properties suggest that $TiB_2$ is a potential reinforcing material for the wear applications where stiffness and high thermal conductivity

*Corresponding author: Tel.: +90 416 2233800; fax: +90 416 2233812; e-mail address: tteker@adiyaman.edu.tr

are important. These properties lead to the titanium and boron use in shields elements. The major advantage is that they eliminate the interfacial incompatibility of matrices with reinforcements by creating more thermodynamically stable reinforcements based on their nucleation and growth from the parent matrix phase. Recently, the in-situ synthesis of $TiB_2$ reinforced metal matrix surfaces composite materials was reported. $TiB_2$ particles were successfully synthesized in microstructures [9]. It is desirable that the surface layer of components is reinforced by $TiB_2$ particles to offer high wear resistance to them whilst they retain the high toughness and strength [10–15].

The objective of this study is to produce a coated surface having maximum amount of $TiB_2$ hard phases with a minimum production cost in a Fe-based surface coating by evenly depositing B, Ti and W based alloy powders and by using the PTA process, and, in addition, to establish relationships between the chemical compositions and microstructure on wear resistance under high stress abrasive conditions.

## 2. Experimental procedures

A powdered mixture of ferroboron (FeB), ferrotitanium (FeTi) and ferrowolfram (FeW) was used as the coating material. Ferro alloys were used as alloying powder due to their price and low melting temperature. Rectangular plates of ferritic stainless steel (AISI 430, 120 mm long, 50 mm wide and 10 mm thick) were used as substrates in the quenched and tempered conditions. The surfaces of the specimens were thoroughly cleaned, dried and finally rinsed with acetone. The main chemical compositions of FeB, FeTi, FeW are listed in Table 1. The average size of the ferro-alloy particulates was less than 50 μm. In order to obtain a homogeneous distribution of particulates, the combined powders were attrition-milled for 1 h using an agate ball mill with an agate container, and the balls were operated at 300 rpm. The milled mixture with a thickness of 1 mm was fed under the plasma arc (Table 2). Coating was conducted to produce a stable arc by using the PTA process and tungsten electrode of 3.2 mm in diameter. Table 3 lists the parameters of the coating process.

The energy given to the surface was controlled as 5 $J\,cm^{-2}$. Specimens were cut from the alloyed specimens for microstructural examination and hardness measurements. The specimens were prepared for metallographic examination by grinding on SiC wheels followed by polishing and etched with a solution of alcohol and 2 % nitric acid. Scanning electron microscopy (SEM) equipped with an energy dispersive X-ray spectrometer (EDS) and X-ray diffraction (XRD) were employed for studying the microstructure and elemental analysis of the coatings. The micro-image analyses with microprocessor were used to determine the hard phase volume fraction and particle size in the coatings. The average hard phase size and volume fraction were determined by quantitative metallography using a digital image analyzer Leica Q550.

The abrasive wear tests were performed by using a pin-on-disc type apparatus. Before the wear tests, each specimen was ground to grade 1200 abrasive paper. Abrasive wear tests were carried out under the load of 10, 20 and 30 N on a grade 80 abrasive paper attached to the grinding disc, which rotated at 320 rev $min^{-1}$. A fixed track diameter of 160 mm was used in all tests, and the duration of the abrasion test was 60 s. Each test was performed with a fresh abrasive paper, and,

Table 1. Chemical concentration of the powders used for coating (wt.%)

| | W | Ti | Si | S | Fe | B | C | P |
|---|---|---|---|---|---|---|---|---|
| FeTi | – | 75 | 0.5 | 0.03 | Bal. | – | – | 0.03 |
| FeB | – | – | 1.5 | 0.04 | Bal. | 80 | 7 | 0.04 |
| FeW | 80 | – | 0.5 | – | Bal. | – | – | 0.04 |

Table 2. Portions of the powders used for coating (wt.%)

| Specimen number | FeTi (%) | FeW (%) | FeB (%) |
|---|---|---|---|
| $S_{1.1}$ | 90 | – | 10 |
| $S_{1.2}$ | 80 | – | 20 |
| $S_{1.3}$ | 70 | – | 30 |
| $S_{1.4}$ | 60 | – | 40 |
| $S_{2.1}$ | 80 | 10 | 10 |
| $S_{2.2}$ | 70 | 10 | 20 |
| $S_{2.3}$ | 60 | 10 | 30 |
| $S_{3.1}$ | 70 | 20 | 10 |
| $S_{3.2}$ | 60 | 20 | 20 |
| $S_{3.3}$ | 10 | 10 | 80 |

Table 3. PTA operating parameters

| Current (A) | Plasma gas flow ($l\,min^{-1}$) | Shielding gas flow ($l\,min^{-1}$) | Traverse speed ($m\,min^{-1}$) | Nozzle diameter (mm) |
|---|---|---|---|---|
| 130 | 0.8 | 20 | 0.01 | 3.2 |

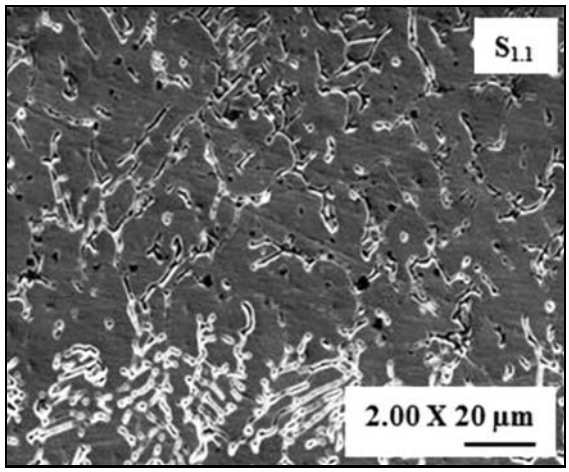


Fig. 1. The SEM micrographs of the coated surfaces of specimen $S_{1.1}$.

for each test condition, a minimum of three runs were performed. Wear rates $W$ ($\mathrm{mm^3\,m^{-1}}$) were obtained by measuring the mass of the specimens before and after wear tests. Wear losses were obtained by determining the mass of the specimens before and after wear tests. The wear rates were calculated by converting the mass loss measurements (to the nearest 0.1 mg) to volume loss by using the respective densities:

$$W\ (\mathrm{mm^3\,m^{-1}}) = \frac{\text{mass loss (g) / density (g mm}^{-3})}{\pi \times 160 \times 10^{-3} \times 320\ (\mathrm{m})}. \quad (1)$$

## 3. Results and discussion

### 3.1. Microstructure of coating

The exothermic dispersion technology [16] was used by applying the PTA to produce a new modified surface in the form of a composite having complex borides ($MB_2$-$M_2B$) reinforcement particulates. This process utilized the melting of the mixture of the ferroalloy powders together with substrate surface under PTA. Melting of these mixtures on the surface of the substrate resulted in exothermal interaction between the components and through these reactions, fine hardening particles could form in the solvent phase as 20–75 vol.%. In some studies [16–18], where Ti-B was used, the reinforcement particulates resulted in the formation of $TiB_2$ with a size of 1–10 µm. Specimen $S_{1.1}$ was coated by FeTi/FeB = 9 ratio. Figure 1 shows the representative microstructures of the coated surface of specimen $S_{1.1}$, where the thickness of modified surface was seen as 1–3 mm.

The X-ray diffraction pattern of the coated surface showed that two types of borides were present, Ti-based and Fe-based borides (Fig. 2). The Fe-based

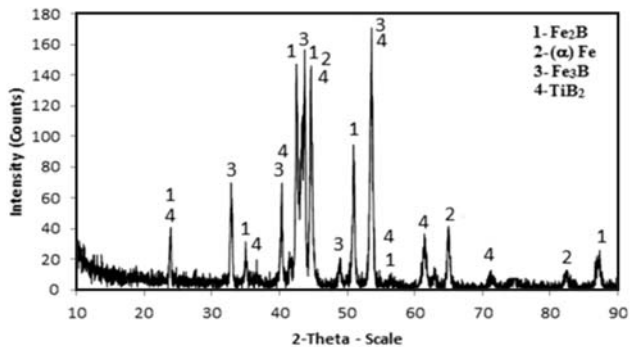


Fig. 2. XRD analyses results of the specimen $S_{1.1}$.

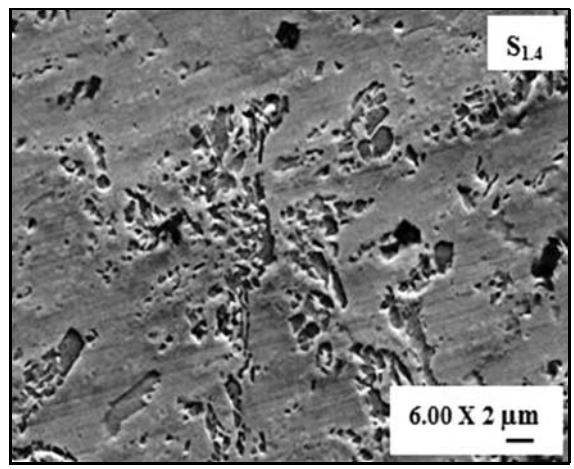


Fig. 3. The SEM micrographs of the coated surfaces of specimen $S_{1.4}$.

borides phase mixture distribution at grain boundaries may be ascribed to the interaction between the particles and the advancing solid-liquid and liquid--liquid interface. During solidification of the molten pool under the arc, the rapid movement of the solid/liquid interface limits in-situ synthesis of $Fe_2B$ particles, and brings about a phase mixture of $Fe_2B$--FeB-$Fe_3B$ borides in an intergranular form. For differentiation of the effect of the chemical concentration of the coating powders on the hard phase ratio, we have decreased FeTi/FeB ratio. This change of coating powder mixture did not affect the morphology of the coated surface microstructure. The increase of the boron at coating solution saturated matrix and diffused boron to grain boundaries during solidification, which then affected the Ti/Fe boride ratio of coating. However, the general microstructures of the first group of the specimens are similar to each other. Figure 3 shows the microstructures of the surface coatings of specimen $S_{1.4}$, on which the matrix is ferrite ($\alpha$-Fe) having $TiB_2$ particulates homogeneously distributed, and the grain boundaries are the Fe borides. It is seen from the elemental distribution that Ti concentration

decreased coming closer from the coated surface to the steel side, on the other hand, $TiB_2$ borides homogeneously distributed inside the matrix phase of $S_{1.2}$ (Fig. 3), and the concentration change of cladding powder material decreased the concentration of Ti in coating surface. Under the PTA, the fine ferroboron particles are melted and merged into streamlets, which arrive at the ferrotitanium particles. During solidification of molten pool, the solidified iron nucleus is surrounded by a thick layer of a crystallized liquid whose composition is close to the composition of the Fe + $Fe_2B$ eutectic melt. Upon solidification of this melt, the Fe, $Fe_2B$, and FeB phases could be found on the corresponding sites of the coating surface (Fig. 3). It is thought that the ferroboron melt covered solid ferrotitanium particles by increasing FeB in volume of coating powder mixture; at the sites of contact, these particles began to penetrate into the FeTi + Ti and $Fe_2Ti$ + Fe eutectics. The figure consists of the FeB grains separated by the eutectic FeB + FeB interlayers at grain boundaries. This shows that boron intensely dissolves in the ferroboron melt, which is a high-boron melt under the PTA. After the ferrotitanium particles are melted completely, the ferroboron and ferrotitanium melts in the coating surface. A layer of titanium diboride continuously forms between the melts, one part of which dissolves as the temperature increases, the other part is carried away by convective liquid flows and is distributed in the form of fine particles in both melts. It seems that the titanium--boron interaction is accompanied by the formation of a contact between $\alpha$-Fe + $TiB_2$. By the moment of crystallization, quite a homogeneous melt forms in the coating surface, which solidifies to form equilibrium $TiB_2$ particles against the background of the $TiB_2$ + Fe eutectic melt. Thus, three types of titanium borides are identified in the final product: primary particles, equilibrium particles and eutectic particles (Fig. 3). In some studies based on Fe-Ti-B systems, (Ti, Fe)$B_2$ and $TiB_2$ phases were detected in the microstructure [16–19], however, we observed basically a $Fe_2B$ phase in the grain boundaries for the first group of the specimens.

The fracture toughness of $Fe_2B$ borides is not sufficient for abrasive wear applications. For this reason, the chemical composition of coating material must be adjusted appropriately to decrease Fe based borides/$TiB_2$ borides ratio [9]. For this reason, ferrowolfram (FeW) was added to the (FeTi + FeB) cladding powder mixture, and the specimens coated by FeTi + FeB + 10 wt.% FeW were called as $S_2$ group (Table 2). The XRD pattern of the surface composite coating of the specimen $S_{2.3}$ is shown in Fig. 4, which indicates that the phases present in the coating are mainly rectangular $TiB_2$, $\alpha$-Fe and $WB_2$ intermetallic compounds, and the micrograph of the coated surfaces of this specimen is given in Fig. 5. The EDS microanalysis showed that there was iron in the titanium boride particles having a changed microstructure. This points to the solid phase character of the initial stage of the titanium boron interaction (Fig. 5). It clearly confirms that $TiB_2$ particulates can be synthesized by a direct reaction between FeTi and FeB in the presence of 10 wt.% FeW, where W was detected at matrix as 0.2 wt.%, and rather it was found as dissolved in hard boride particulates as 0.6–0.7 wt.%. The results show that the intermetallic compounds form dendritically during the late stages of solidification. A small change of Ti/B ratio changes the chemical composition of liquid solution, causing a shift in the structure from $TiB_2$-Fe binary phase equilibrium to $TiB_2$-Fe--$Fe_2B$ [20]. This hypothesis was approved; the chemical composition of Ti in $TiB_2$ phase decreased from 78 to 40 wt.% by decreasing the FeTi powders in cladding powder from 80 to 70 wt.% (Table 2).

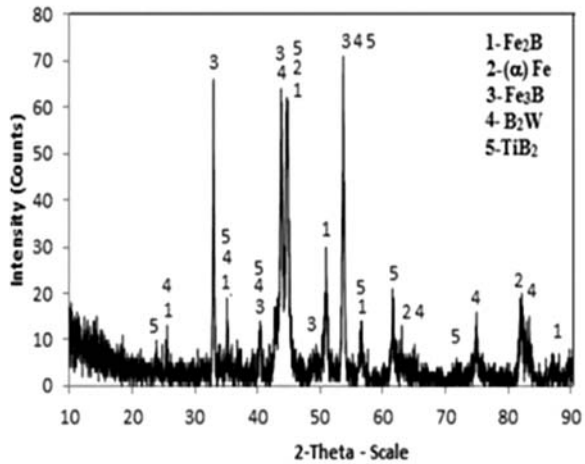


Fig. 4. XRD analyses results of the specimen $S_{2.1}$.

As described, it is thought that the solidification systematic of the first group of the specimens is similar to the second group of the specimens. By using the considered solidification sequence, one can determine the processes in the coating of the second group of specimens from the metallographic results. The final product is a result of the solidification of the melt, as in the first case, the appearance of the liquid phase in the coating is due to the contact melting of the charge components and substrate. When considering the structure formation in the coating, we assumed that the liquid phase formed on the sites of coating powder particles contact as a result of contact melting according to the diffusion-free mechanism. It implies that the following two factors are sufficient for the liquid phase to appear in the coating: the contact between the powder particles and the corresponding temperature [8]. The liquid phase forms at the sites of contact between the ferrotitanium and ferroboron particles. The first portions of the liquid

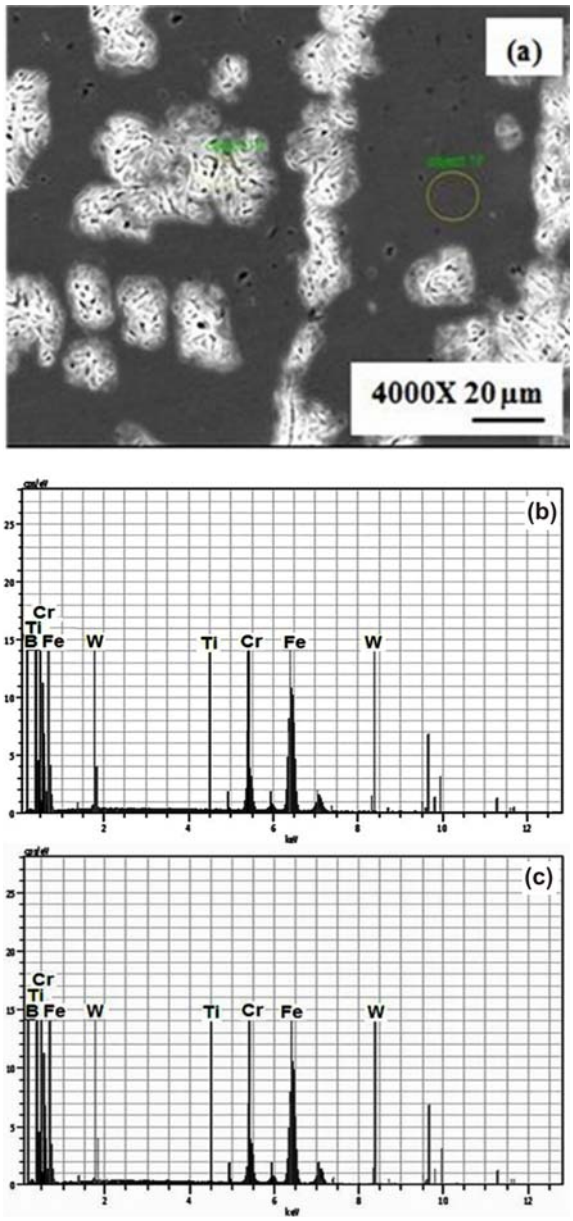


Fig. 5a,b,c. The SEM micrographs and EDS microanalysis of the coated surfaces of specimens $S_{2.3}$.

phase appear in the system when the temperature corresponds to the FeTi low-temperature eutectic melt. Possibly, when the temperature corresponding to the second $Fe_2Ti$ + Fe eutectic melt is reached, the liquid phase of another composition forms at the contact sites. After the appearance of the liquid phase in the system, the ferroboron-ferrotitanium interaction occurs via the contact melt in which iron, boron, titanium and wolfram dissolve as the temperature increases. When the liquid phase forms a partial disperse on of ferroboron, ferrotitanium and ferrowolfram particles are observed. The fine initial and dispersed FeB particles dissolve rapidly in the ferrotitanium

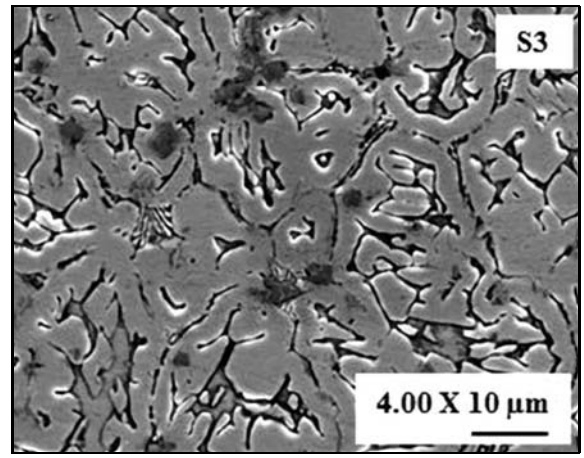


Fig. 6. The SEM micrographs of the coated surfaces of specimen $S_3$.

melt, saturating it with wolfram and boron. The ferroboron particles are gathered by the contact melt in the molten pool. At the interface between these particles and the melt, the $TiB_2$ layers form. Ferrotitanium dissolves completely in the intermediate melt, which contacts extensively with the rest of the ferroboron particles. In Fig. 5, the ferroboron regions bordering the melt are light coloured. As the analysis shows, these are the regions of almost pure iron which were formed as a result of the intense diffusion of boron into an "intermediate" melt. The Fe-borides and the grain interfaces, where the diffusion flows primarily occur, are depleted of boron, too. After the rest of the ferroboron has melted completely through the intermediate melt, near the region, a concentration-inhomogeneous melt forms; this melt crystallizes to yield titanium borides and several types of structure: $W_2B_5$, $WB_2$, $W_2B$, FeWB, $WB_4$ and $Fe_3B$.

Regarding the third group, the concentration of the FeW in coating powders increased from 10 to 20 wt.%. In other words, the specimens coated with cladding material containing FeTi-20wt.%FeW-FeB were called as $S_3$ group. The SEM micrographs of the coated surface of the $S_3$ group specimens that were coated with cladding powders mixture of the FeTi-FeW--FeB are given in Fig. 6. As seen from the microstructure, W was significantly dissolved in the matrix (Fig. 7). The existing phases of the coated surface of the third group are mainly $TiB_2$, $WB_2$ and $\alpha$-Fe (Fig. 7). The intermetallic compound $Fe_2B$ was not observed for the specimens coated by FeW-FeB-FeTi powders mixture. The $TiB_2$ phase was formed homogeneously and in rectangular form. The diborides of IV-VI group metals dissolve at temperatures of 2000–3000 °C, and the atomic size difference between the elements decreases the dissolution temperatures [20]. For this reason, it is thought that W activated the formation of (Ti, Fe)$B_2$. The analysis shows that the

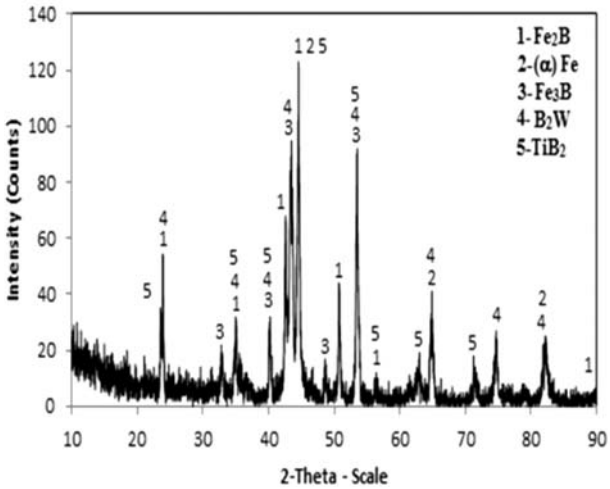


Fig. 7. XRD analyses results of specimens $S_{2.3}$.

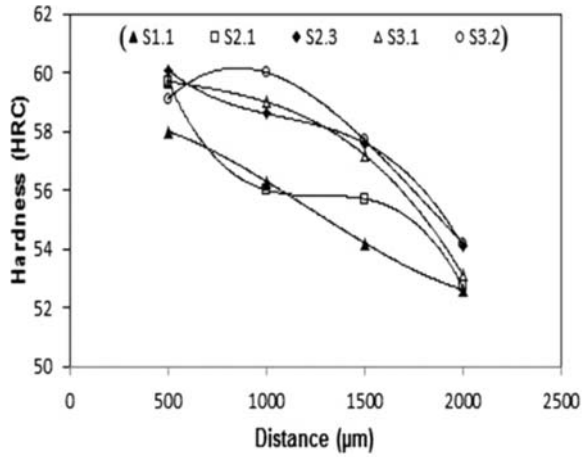


Fig. 8. Hardness via layer depth of the PTA processed coating.

Table 4. EDS analysis taken from the surface of sample $S_{2.3}$

| | B | Ti | Cr | Fe | W |
|---|---|---|---|---|---|
| Matrix | 3.83 | 0.21 | 14.96 | 77.10 | 3.90 |
| Fe-Boride wt.% | 5.01 | 0.28 | 13.60 | 63.41 | 1.02 |

hard particulates are (Ti, Fe)$B_2$ when the concentration of cladding powders is about 70 wt.% FeTi. But the decrease of FeTi powder concentration in cladding powders from 70 to 60 wt.% changed the type of the boride from (Ti, Fe)$B_2$ to (Fe, Ti)$_2$B. Depending on the elemental analysis, Ti wt.% at hard particulates is 65, 19.23 and 3.61 for specimens $S_{3.1}$, $S_{3.2}$, $S_{3.3}$, respectively. Depending on these changes, one can infer that the concentration of the FeTi in cladding powder mixture has determinative effect on the formation of titanium diboride. The $TiB_2$ phase can be present together with FeB, $Fe_2B$, $\alpha$ or $\gamma$-Fe, $FeTi_2$ and FeTi phases, and the borides which were formed by transition metals have lower melting temperatures [20]. The specimens coated with W have shown that W decreased the total hard phase ratio; on the other hand, $TiB_2$ ratio in hard phases increased. Three types of borides: (Ti, W)$B_2$, (Ti, W)$B_2$ and (W, Ti)$_2B_5$, can form at Ti-W-B system [19]. However, (Ti, W)$B_2$ phases were not observed in specimens $S_{3.1}$-$S_{3.2}$-$S_{3.3}$ in this work. The best material balance for maximum $TiB_2$ and minimum $FeB_2$ phases was seen as the composition of $S_{3.2}$.

### 3.2. Hardness of the coating

The hardness of the coated surface reinforced by $TiB_2$, $WB_2$ and $Fe_2B$ borides was determined along the depth of the irradiated surface; all the data was an average of three measurements. The variations of the hardness across the transverse cross section of the coating are presented in Fig. 8 demonstrating that the presence of FeW and FeTi in the coated surface produce an increase in hardness. The hardness of the coating progressively decreased from the surface to the substrate. It is noted that there is no sudden transition from the coating to the substrate in the hardness, which indicates an absence of a sharp demarcation in materials properties across the interface. Furthermore, the average hardness of the coating gradually increased with an increase in the content of $TiB_2$ and $Fe_2B$, which was partly due to the formation of more particles during PTA processing. The highest hardness value was obtained from the coated specimen having 39 vol.% hard phase ratio. The matrix hardness also changed depending on the chemical concentration. The reported hardness value of $TiB_2$ varied from 2900 HV [21] to 3400 HV [22]. The measured hardness value of $TiB_2$ fell within the reported range. The measured hardness of $Fe_2B$ matches with the literature value [22–24].

### 3.3. Wear characterization of the coatings

The effect of the load on the wear rate of the specimens is given in Fig. 9a–d. The figure emphasizes the role of applied load between wear rate and loading in a polynomial function. The specimen $S_{2.1}$ shows the lowest wear rate for the second group of the specimens (Fig. 9b), and the specimen $S_{3.1}$ shows the lowest wear rate for the third group of the specimens (Fig. 9c). The wear rate of the specimens did not change in a great difference, and between the three groups of the specimens, the lowest wear rate was seen for the specimen $S_{3.1}$. The wear rate of the specimens was increased by the decrease of the FeTi/FeB rate of the

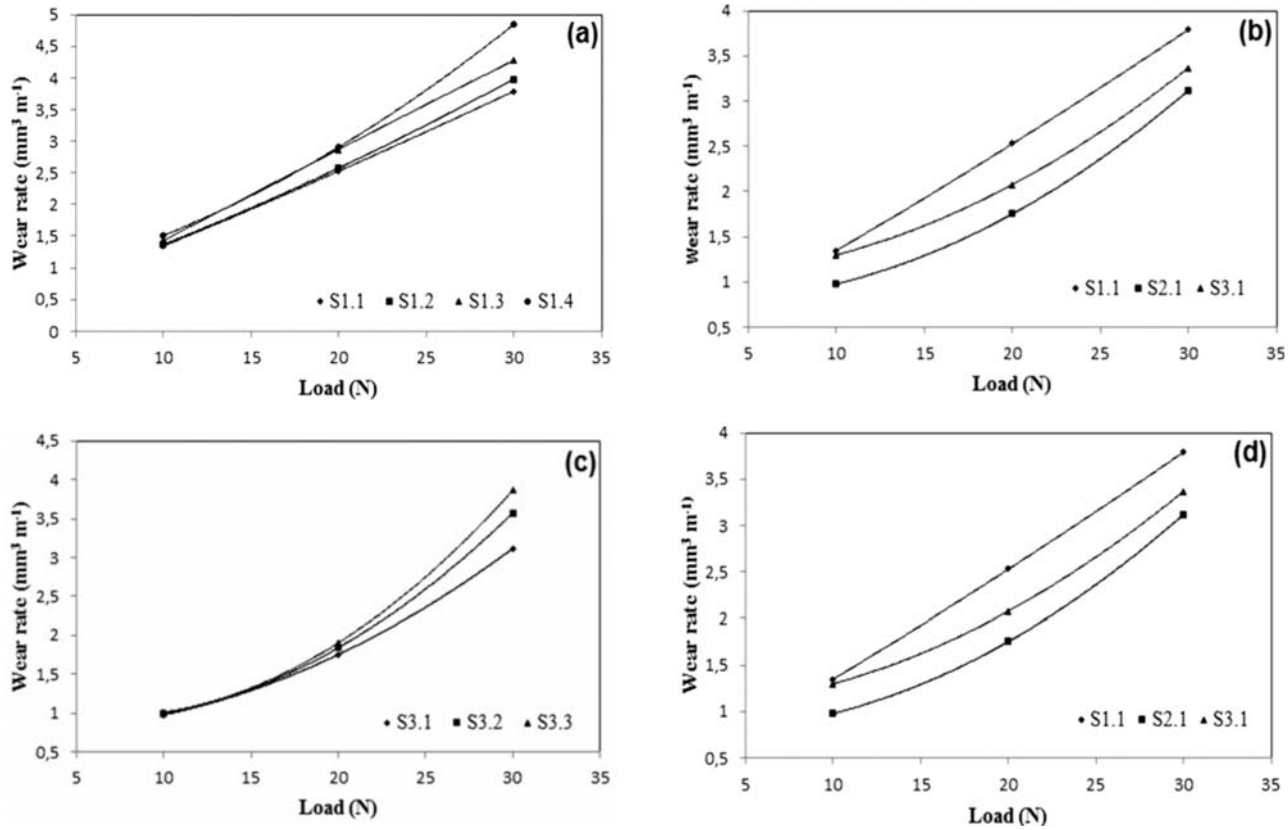


Fig. 9. The effect of the load on the wear rate of the specimens: a) $S_1$ group, b) $S_2$ group, c) $S_3$ group, d) comparison of the groups.

coating powders, and the addition of the FeW to cladding powder mixture FeTi + FeB decreased wear rate of the coated surfaces (Fig. 9d).

The wear resistance of a composite surface depends on hardness, microstructural parameters (volume fraction, size, shape, and distribution of embedded particles, properties of matrix), and the interfacial bonding between the phases [24]. The overall depth of the plastic deformation of coated surface under the abrasive grits during wearing related linearly to the applied load and the grit dimensions. Furthermore, the tribological behavior of a coated surface depends on the microstructural properties of the surface and the type of loading-contact situation [5]. Behind these tribo-mechanical situations considering Fig. 9, the specimen $S_{1.1}$ having the highest Ti concentration in matrix of coated surface demonstrates a lower wear rate than other specimens in the first group of specimens. The deviation of the wear rate for the first group of the specimens is attributed to the content of boron/titanium ratio and the boride vol.% with the boride size.

The relationship between the wear rate and the boride properties of the coated surfaces is given in Fig. 10a,b,c. The wear rate decreases with an increase on Ti level in hard phases, and this means that the wear rate decreases with increase of boride volume fraction and boride size. A comparison between the change of Ti in the matrix of the specimens shows that a significant increase in the Ti concentration promotes the formation of thicker and harder coatings and melted regions over the substrate. The decrease of the FeTi concentration in coating powders decreased boride vol.%, boride size and Ti wt.%, where these three ingredients increased the wear rate (Fig. 10c). Among these parameters, it will be difficult to determine the most effective major factor on the wear rate, but depending on the change of the hard phase ratio (from 40 to 25 vol.%), it can be said that the change of FeTi/FeB ratio is more predominant on the wear rate by changing the hard phase ratio. The change of the cladding powder concentration affected the type and vol.% of the borides. It is supposed that the mechanical and tribological properties of the coatings having boride reinforcement structure depend strongly on the hard phase ratio with boride distribution and the chemical concentration change, whereas the wear behavior operates differently depending on the orientation of the borides with respect to the wear surface of coating. In the coated surface of the specimens, having the borides oriented transverse to the abrasion direction, and with the long axis of the borides perpendicular to the wear surface, the borides bend and fracture very near the surface. In this case, it was considered

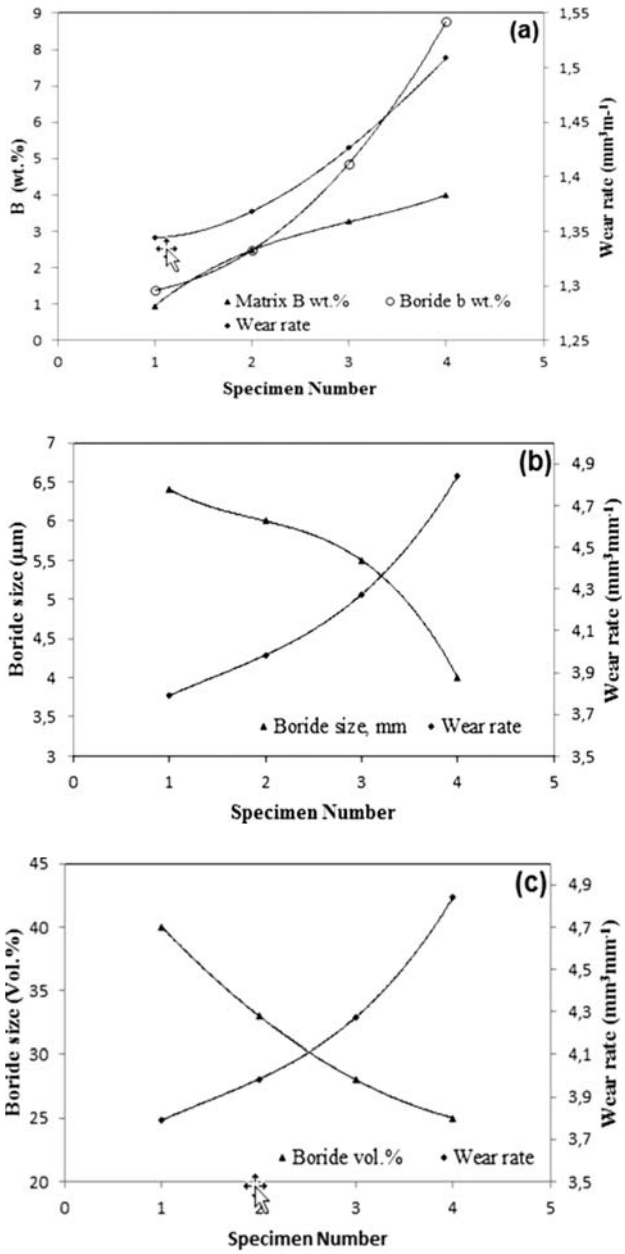


Fig. 10. The relationship between a) wear rate versus boron wt.%, b)wear rate-boride size, c) wear rate-boride vol.% for the sample $S_{1.1}$-$S_{1.4}$.

that the tangential forces applied by the moving abrasive particles caused bending. During bending, tensile stress develops on the backside of boride, leading to fracture. However, as the boride size decreases, bending and fracture become more difficult under the same applied tangential force. Both the $TiB_2$ and $Fe_3B$ hard phases may act as reinforcements in the composite like coated surface, and the increase of the boride size decreased wear rate in a parabolic function (Fig. 10b).

Harder borides ($TiB_2$) in the coated structures appear more resistant to deformation and fracture during wearing, which emphasizes that the concentration of the borides changes at the coating matrix of the specimens, and the difference of the boride concentration has brought a difference in wear behavior, it has changed from matrix to the borides. It is considered that the abrasive wear results can form an opinion about the effect of the boride volume fraction on the wear behavior and wear resistance of the coated surfaces [9]. We have seen that the boron wt.% of the borides have not an effect on the wear rate alone. The effect of the size of the borides must be considered as well. The surfaces having high $TiB_2$ and low $Fe_2B$ are expected to be more resistant to abrasion. It can be concluded that the boride structure in these coated surfaces is un-influential on abrasive tribo-environment. In addition, the nature of the matrix surrounding the boride has also a profound effect on the performance of borides. The results of this study clearly demonstrate that the orientation of borides in the wear of specimens having $TiB_2$ and $Fe_2B$ microstructure influences the wear rate significantly. The hardness of $TiB_2$ particles in the surface is higher than 3000 HV. Khrushov et al. [25] suggest that the higher is the hardness of the reinforcing particle, the better the wear resistance is. As seen from the wear rates of the specimens and the surface hardness of the specimens, a qualitative difference was not found between the hardness and the wear rates. But the wear rate of the specimens having hard matrix suggests less sensitivity to the load (Figs. 8, 9d). The delay of the load effect can be attributed to the presence of hard phases and their vol.%. On the other hand, the hard reinforcements have the deleterious effect on the wearing the counter face more than the unreinforced material. In addition, spalls detached from cracks might propagate and behave as third-body abrasion, worsening wear behavior. The micrographs of the wear surfaces of the specimen $S_{1.1}$ and $S_{3.1}$ are given in Fig. 11a,b to compare the size of the wear debris of the best and worst wear resistant specimens. From the wear debris of the specimens it is seen that the size of the debris is not different desperately. For this reason, it is thought that the impact strength of the hard phase has an effect on the wear results.

## 4. Conclusions

1. The formation of the $Fe_2B$ in the microstructure decreased the wear rate significantly. The wear rate of the specimens was increased by the decrease of the FeTi/FeB ratio in the coating powders.

2. The usage of FeW powders together with FeTi and FeB activated formation of $TiB_2$, and formed mainly spherical $TiB_2$ and interdendritical $Fe_2B$ as $\approx$ 30 vol.% $TiB_2$.

3. The increase of the FeW/(FeB + FeTi) ratio in cladding powder dissolved Ti and W in the matrix,

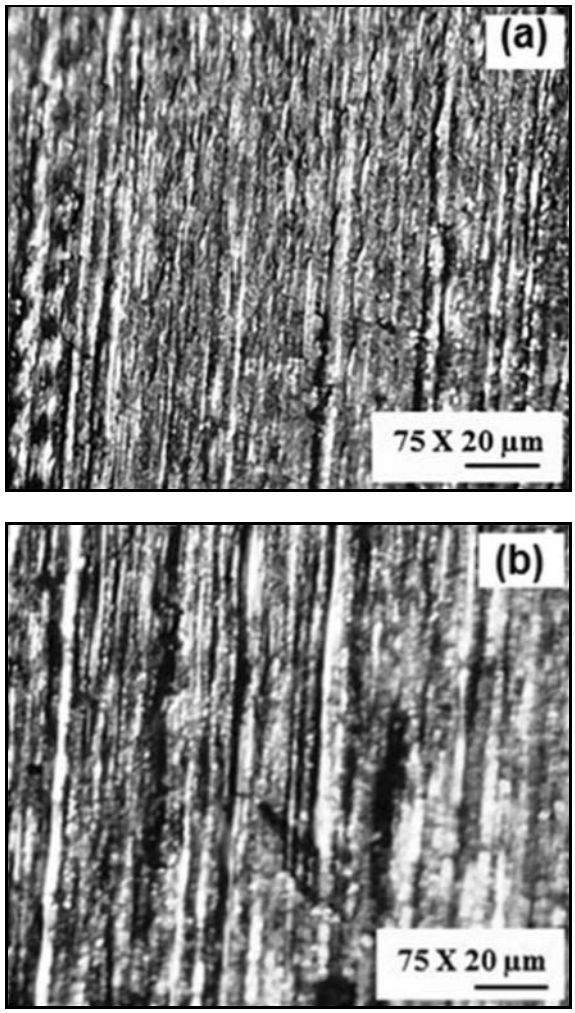


Fig. 11. a) Wear micrograph of specimen $S_{1.1}$, b) specimen $S_{3.1}$ (X75).

and $TiB_2$ and $Fe_2B$ phases enhanced the hardness of the coatings.

4. The highest $TiB_2$ vol.% was obtained from the specimen coated by 20 FeW + 60 FeTi + 20 FeB cladding powders mixture.

4. The presence of the FeW in the cladding powders with FeB + FeTi decreased wear rate, and the best wear resistance was obtained for the specimen coated by a powder having (20 FeW + 60 FeTi + 20 FeB).

5. The decrease of the wear rate by addition of FeW to FeTi-FeB is attributed to the presence of B wt.% in matrix, the increase of vol.% and size of the borides.

## References

[1] Liu, Y. F., Mu, J. S., Xu, X. Y., Yang, S. Z.: Materials Science Engineering A, *458*, 2007, p. 366. doi:10.1016/j.msea.2006.12.086

[2] Deuis, R. L., Yellup, J. M., Subramanian, C.: Sci. Technol., *58*, 1998, p. 299.

[3] Tsay, L. W., Lin, Z. W., Shiue, R. K., Chen, C.: Materials Science Engineering A, *290*, 2000, p. 46. doi:10.1016/S0921-5093(00)00950-3

[4] Tian, X., Chu, P. K.: Scripta Mater., *43*, 2000, p. 417. doi:10.1016/S1359-6462(00)00436-X

[5] Holmberg, K., Matthews, A., Ronkainen, H.: Tribology International, *31*, 1998, p. 107. doi:10.1016/S0301-679X(98)00013-9

[6] Fu, Y. G., Wei, J., Batchelor, A. W.: Journal of Materials Processing Technology, *99*, 2000, p. 231. doi:10.1016/S0924-0136(99)00429-X

[7] Zapponi, M., Quiroga, A., Pérez, T.: Surface and Coating Technology, *122*, 1999, p. 18. doi:10.1016/S0257-8972(99)00403-X

[8] Hadfield, R. A.: Metallurgy and Its Influence on Modern Progress. London, Chapman and Hall, Ltd. 1925.

[9] Modenesi, P. J., Apolinario, E. R., Pereira, I. M.: Journal of Materials Processing Technology, *99*, 2000, p. 260. doi:10.1016/S0924-0136(99)00435-5

[10] Zeng, Z. M., Zhang, T., Tang, B. Y., Tian, X. B., Chu, P. K.: Surface and Coating Technology, *120*, 1999, p. 659. doi:10.1016/S0257-8972(99)00427-2

[11] Cahn, R. W.: The Encyclopedia of Ignorance. New York, Pergamon Press 1977.

[12] Raghavan, V., Raghavan, K. S., Sastri, S. A., Marcinkowsky, M. J.: Transactions of the metallurgical society of AIME chapter part VII – Nature of the work-hardening behavior in hadfield's manganese steel, 1969, p. 1299.

[13] Stringer, J.: Surface and Coating Technology, *1*, 1998, p. 108.

[14] Panagopoulos, C. N., Markaki, A. E., Agathocleous, P. E.: Materials Science Engineering A, *241*, 1998, p. 226. doi:10.1016/S0921-5093(97)00495-4

[15] Smith, R. W., De Monte, A., Mackay, W. B. F.: Journal of Materials Processing Technology, *153*, 2004, p. 589. doi:10.1016/j.jmatprotec.2004.04.136

[16] Goldfarb, I., Bamberge, M.: Scripta Mater., *34*, 1996, p. 1051. doi:10.1016/1359-6462(95)00622-2

[17] Zeng, Z., Zhang, J.: Surface and Coating Technology, *202*, 2008, p. 2725. doi:10.1016/j.surfcoat.2007.10.008

[18] Satyaprasad, K., Mahajan, Y. R., Bhanuprasad, V. V.: Scripta Mater., *26*, 1992, p. 711. doi:10.1016/0956-716X(92)90425-E

[19] Petzow, G., Telle, R., Danzer, R.: Materials Characterization., *26*, 1991, p. 289. doi:10.1016/1044-5803(91)90018-Y

[20] Nishiyama, K., Umakawa, S.: In: Proc. 5th Japan-US Conference on Composite Materials. Ed.: Kobayashi, A. The Japan Society of Composite Materials. Tokyo, 1990, p. 371.

[21] Hilz, G., Holleck, H.: Materials Science Engineering A, *139*, 1991, p. 268.

[22] Terry, B. S., Chinyamakobvu, A. S.: Materials Science Technology, *8*, 1992, p. 491. doi:10.1179/026708392790170928

[23] Degnan, C. C., Shipway, P. H.: Metallurgical Materials Transaction A, *33*, 2002, p. 2973.

[24] Pagounis, E., Talvitie, M., Lindroos, V. K.: Powder Metallurgy, *40*, 1997, p. 55.

[25] Khruschov, M. M.: Wear, *69*, 1974, p. 69. doi:10.1016/0043-1648(74)90102-1